STUDIES OF KILOPARSEC-SCALE, STEEP-SPECTRUM RADIO CORES. I. VLA MAPS

WIL VAN BREUGEL[a)]
Steward Observatory, University of Arizona, Tucson, Arizona 85721

GEORGE MILEY[a)]
Leiden Observatory, Postbus 9513, 2300 RA Leiden, The Netherlands

TIMOTHY HECKMAN[a)]
Astronomy Program, University of Maryland, College Park, Maryland 20742
Received 19 July 1983; revised 27 September 1983

ABSTRACT

VLA maps with resolution of 0.15″–0.4″ are presented of the structures and polarization distributions of several of a sample of 23 powerful sources (mostly quasars) with dominant structure on the kiloparsec scale. The radio properties of these "steep-spectrum core" (SSC) sources (generally: low percentage polarization, complex morphology, kiloparsec size, and high surface brightness) resemble those of the weaker, nearby SSC's such as found in some Seyferts (i.e., NGC 1068) and in sources like 3C 293, 3C 305, M87, and 4C 26.42. Previous studies of nearby SSC's have shown that these are embedded in gas-rich environments as evidenced by their associated optical narrow-line regions (NLR's) and rotating gaseous disks, dustlanes, neutral hydrogen, or cooling galactic coronae. The similarities of the radio properties of nearby and distant SSC's and recent optical evidence that many quasars may reside in spiral-type, and hence gas-rich, galaxies suggest that quasar SSC's are also embedded in relatively dense interstellar media and have associated NLR's. Many of the radio and optical properties of SSC's may thus be understood as being due to the interaction of jets with their dense environments.

I. INTRODUCTION

There are two well-known types of emission from extragalactic radio sources. Extended radio components with steep spectra and typical sizes >100 kpc and compact nuclear components with flat spectra and sizes <1 pc. During the last few years a third class of radio source components has been discovered having a characteristics scale of ~ 1 kpc. These kiloparsec-scale components are associated with the nuclei of their parent galaxies and have steep radio spectra. They have been christened steep-spectrum cores (SSC's) (Bridle and Fomalont 1978; Miley 1980).

Here, we shall define a SSC as a radio source component which has a spectral index of $\alpha > 0.5$ ($S_\nu \sim \nu^{-\alpha}$) in the frequency range of at least 1 GHz–15 GHz and which has a linear size smaller than a typical galaxy diameter (<25 kpc; throughout this paper we will assume a value for the Hubble constant of 75 km s^{-1} Mpc^{-1} and a deceleration parameter $q_0 = 0.5$). Thus defined SSC's sometimes occur in combination with very extended and/or compact radio emission, either component of which may dominate. SSC's with very extended radio emission are, for example, 3C 293 (Bridle *et al.* 1981) and 3C 236 (e.g., Schilizzi *et al.* 1981). There are also sources whose radio emission is primarily due to SSC's such as in the galaxies NGC 1068 (e.g., Wilson and Ulvestad 1983), M87 (e.g., De Young *et al.* 1980), 3C 305 (Heckman *et al.* 1982), and in the quasars 3C 48, 3C 138, and 3C 147 (Donaldson *et al.* 1971).

SCC's are of particular interest because they have similar sizes to those of the narrow (forbidden) line regions (NLR's). There are suggestive correlations linking the SSC radio luminosities with both the NLR [O III] λ 5007 luminosities (de Bruyn and Wilson 1978) and the NLR [O III] λ 5007 linewidths (Wilson and Willis 1980; Heckman *et al.* 1981).

In general, nearby SSC's are associated with relatively gas-rich galaxies: Seyferts (such as NGC 1068), peculiar galaxies with rotating gaseous disks and dustlanes (3C 305, 3C 293, NGC 3801) and/or neutral hydrogen (3C 293, NGC 1167, NGC 3801; see Heckman *et al.* 1983) or cooling x-ray coronae (M87, see Ford and Butcher 1979 and De Young *et al.* (1980); 4C 26.42, van Breugel *et al.* 1983b). In addition, in several of these cases there is direct morphological evidence for interaction between the SSC's and their environment (see also van Breugel and Heckman 1982).

More distant quasar-SSC's may be more powerful but otherwise similar objects. For example, optical imaging of nearby quasars suggests that a fair fraction of them (perhaps more than 30%) may reside in spiral-type and hence gas-rich galaxies, possibly in the process of merging with companions and thereby triggering the quasar activity (e.g., Hutchings and Campbell 1983). In the case of 3C 48, where the NLR is spatially resolved, it extends roughly in the same direction as the SSC and spectroscopically the underlying galaxy resembles a spiral (e.g., Boroson and Oke 1982).

Many of the radio and optical properties of SSC's may thus be understood as being due to jets propagating through dense interstellar media (see, for example, Heckman *et al.* 1982; van Breugel 1983a, b). We have begun a detailed radio and optical investigation of such objects and VLA observations of a sample of distant, powerful SSC's are the subject of the present paper. These observations show that also the radio properties of these objects resemble those of the nearby and weaker SSC's.

We have used the VLA in its highest resolution mode (A configuration, Thompson *et al.* 1980) to obtain radio intensity and polarization distributions for a sample of SSC sources at λ 2 cm (0.15″ resolution). Some sources were also observed at λ 6 cm (0.4″ resolution). The sample included all SSC's listed by Peacock and Wall (1982; henceforth PW) with mea-

[a)] Visiting Astronomers at the National Radio Astronomy Observatory, which is operated by the Associated Universities, Inc., under contract with the National Science Foundation.

 0004-6256/84/010005-18$00.90

TABLE I. Observing log and general information.

Source	Other Name	λ 2 cm Number of Scans	λ 2 cm Total Observing Time (min)	λ 6 cm Number of Scans	λ 6 cm Total Observing Time (min)	Object Type	Redshift	Visual Magnitude	Spectral Index 6cm - 21cm	Log $P_{1.4}$ (WHZ^{-1})	Total Linear Size (Kpc)	Comments
(1)	(2)	(3)		(4)		(5)	(6)	(7)	(8)	(9)	(10)	(11)
0116+319	4C 31.04	1	10	-	-	G	0.0590	14.5	0.43 P	25.21	< 0.03	P
0134+329	3C 48	2	6	-	-	Q	0.367	16.2	(0.79) P	27.61	3.5	P, L
0221+276	3C 67	3	30	3	13	G	0.3102	18	0.95 K	26.79	8.2	PH
0429+415	3C 119	1	10	-	-	Q	0.408	20	0.70 P	27.46	0.2	Not in PW SSC Sample. P, PRW
0518+165	3C 138	3	11	3	8	Q	0.759	17.9	0.67 P	28.05	4.5	P, L
0538+498	3C 147	2	8	-	-	Q	0.545	17.8	0.85 P	28.16	4.4	P, L, S
1117-248	-	1	9	-	-	Q	0.466	17.1	0.73 P	26.88	1.3	Not in PW SSC Sample. P
1153+317	4C 31.38	1	10	1	4	Q	1.557	19.0	0.90 K	28.30	6.8	PW
1203+645	3C 268.3	1	10	1	4	G	0.422	20.0	0.97 K	27.17	6.1	L
1250+568	3C 277.1	1	10	1	3	Q	0.321	17.9	0.69 K	26.71	5.8	PH
1328+254	3C 287	2	10	-	-	Q	1.055	17.7	0.61 P	28.19	0.3	P
1328+307	3C 286	4	16	4	10	Q	0.846	17.3	0.55 P	28.30	14.1	P, L, S, PRW
1345+125	4C 12.50	1	10	-	-	G	0.1218	17.0	0.49 P	26.17	0.3	P
1354+196	4C 19.44	-	-	4	10	Q	0.720	16.0	0.16 P	-	--	Not a SSC. Extra phase calibrator.
1419+419	3C 299	1	10	1	3	G	0.367	19.4	0.93 K	26.93	23.5	L
1437+624	-	1	10	-	-	Q	1.090	19.0	0.80 P	27.79	0.7	Not in PW SSC sample. P
1442+101	OQ 172	1	10	-	-	Q	3.530	17.6	0.60 P	28.78	< 0.1	P, MS
1458+718	3C 309.1	5	24	1	4	Q	0.904	16.8	0.64 K	28.15	12.2	KWB, L
1629+680	4C 68.18	1	10	-	-	Q	2.475	18.7	0.66 P	28.04	0.5	Not in PW SSC sample. P
1634+628	3C 343	1	10	-	-	Q	0.988	20.6	(0.96) P	28.08	0.3	P
1637+626	3C 343.1	1	10	-	-	G	0.750	20.8	1.10 P	27.81	1.4	P
1901+319	3C 395	1	10	1	3	Q	0.635	17.5	0.48 P	27.27	3.6	Not in PW SSC sample. P, PM
2230+114	CTA 102	1	10	-	-	Q	1.037	17.3	0.34 P	(28.04)	< 0.06	Highly variable source. P, PRW, L
2247+140	4C 14.82	2	20	-	-	Q	0.237	17.0	0.47 P	26.31	1.2	P

sured redshifts (18 objects). To this list we added five sources from the VLA calibrator list (Perley 1982) also having a steep spectrum ($\alpha_{21}^{6} > 0.5$) and known redshifts. In addition to the observations at λ 2 cm we observed six sources at λ 6 cm for which no good maps were available at that wavelength.

Our observations of the SSC's from PW's sample with a visual magnitude < 17.5 would formally constitute a complete subsample using their definition of SSC's (smaller than 2″–3″ at 2.7 GHz and $\alpha_{11}^{6} > 0.50$). Such a definition may not be very physically meaningful, however, since nearby SSC's and SSC's which have also extended emission are being discriminated against due to their larger *angular* sizes (van Breugel 1983). Moreover, the spectral index is defined over a rather narrow frequency range which results in the inclusion of objects with complex spectra. Also the variability of certain objects may bias the sample. This may explain, for example, why seven sources with steep spectra in PW's list have spectral indices much smaller than 0.50 when data over a larger spectral range are included. These sources are: 0116 + 31, 0319 + 12, 0428 + 20, 1150 + 49, 1600 + 33, 1749 + 70, and 2230 + 11 (see Perley 1982 and Kuhr *et al.* 1981).

II. OBSERVATIONS AND REDUCTION

The observations were made on 24 and 26/27 February 1982 with the VLA in its highest resolution (A) configuration. All sources were observed at λ 2 cm (14 965 MHz) and nine additional sources were observed at λ 6 cm (4885 MHz). A bandwidth of 50 MHz was used in both cases. The number of scans and the total integration time for each source is given in Table I, together with some other general information. Listed are:

Column *1.* Source name, IAU designation.
2. Other source name.
3. Number of scans at λ 2 cm and total time on source at this wavelength.
4. The same for λ 6 cm.
5. Object type. G = galaxy, Q = quasar.
6. Redshift.
7. Visual magnitude.
8. Spectral index between λ 6 cm and λ 21 cm taken from Perley (1982; P) or, if not in that catalog, derived from Kuhr *et al.* (1981; K).
9. The log of the power at λ 21 cm assuming $H_0 = 75$ km s^{-1} Mpc^{-1} and $q_0 = 0.5$.
10. Total linear size in kiloparsecs.
11. Comments. Recent high-resolution observations by other authors are referred to as: P = Perley (1982); L = Laing (1981); PH = Pooley and Henbest (1974); PRW = Pearson *et al.* (1980); S = Simon *et al.* (1980); PW = Peacock and Wall (1982); MS = Marscher and Shaffer (1980); KWB = Kus *et al.* (1981); PM = Phillips and Mutel (1980).

The optical information was taken from the catalogs by Burbidge and Crowne (1979) and Hewitt and Burbidge (1980), except for 3C 395 (Wills and Wills 1979).

The data were calibrated by the VLA staff. The absolute amplitude and polarization position angle calibration was based on 3C 286. Since this source is resolved on the longest baselines, only the shortest baselines were used to obtain bootstrapped flux densities of other program sources which had only very weak secondary structure (0116 + 319, 0429 + 415, 1442 + 101, 1458 + 718, 1901 + 319, 2230 + 114 at λ 2 cm; 1901 + 319 at λ 6 cm). These sources and 1354 + 196 (at λ 6 cm; not a program source) were used as phase and amplitude calibrators. Instrumental polarization was calibrated using 1458 + 718 (λ 2 cm) and 3C 286 (λ 6 cm).

Weather during the observations was bad (storms, rain) which resulted in somewhat less accurate absolute positions at λ 2 cm than might otherwise have been possible. By comparing the positions (flux-weighted averages in the case of sources with multiple components) with those known at λ 6 cm (Perley 1982), we estimate that the uncertainties of the absolute positions are < 0.2″. At λ 6 cm the uncertainties in our observations are probably < 0.1″.

Further data processing was done using the NRAO software at the VLA and the NRAO/WSRT combined reduction system in Leiden. After Fourier transformation, maps were made using a 256 × 256 grid and pixel sizes of 0.03″ (λ 2 cm) and 0.1″ (λ 6 cm). The inner quarter of the maps was cleaned so that secondary structure further away than 3″ (λ 2 cm) and 12.8″ (λ 6 cm) from the central object would be missed. The sampling of the source structure in the A configuration is such that no larger scale structure than 4″ (λ 2 cm) and 11″ (λ 6 cm) would be detectable in our maps.

To facilitate the interpretation all the cleaned maps were restored using circular Gaussian beams with a full width at half-maximum of 0.15″ (λ 2 cm) and 0.4″ (λ 6 cm). These represented the actual beam sizes fairly well since all sources were observed close to the meridian.

All maps were self-calibrated using several iterations until no further improvement could be obtained. The final noise (confusion) levels reached were typically 3 mJy/beam (λ 2 cm) and 1.7 mJy/beam (λ 6 cm).

Sizes and flux densities of individual source components were determined using a Gaussian fitting program. Visibility amplitude plots of sources with single components allowed a partial check on these results. In all these cases the Gaussian fits and the variation of the visibility amplitude as a function of distance in the Fourier plane appeared consistent. In a few cases Gaussian fits could not represent the source structure very well, as indicated in Tables II and III.

III. RESULTS

Some general information on the sources is summarized in Table I (see Sec. II for details).

The positions, sizes, flux densities, and polarization parameters are given in Table II (λ 2 cm) and Table III (λ 6 cm). Listed are:

Column *1.* Source name, IAU designation.
2. Other source name.
3. Source component.
4. Right ascension (1950).
5. Declination (1950).
6,7,8. Component size (major axis, minor axis, position angle).
9. Flux density as determined by Gaussian model fits.

TABLE II. 2-cm parameters.

Source	Other Name	Component	RA(1950) H M S	DEC(1950) D M S	Major Axis (arcs)	Minor Axis (arcs)	PA (deg)	Flux Density (mJy/beam)	Polarization %	Polarization PA	Peak Total Intensity (mJy/beam)	rms Noise (mJy/beam)	Comments
(1)	(2)	(3)	(4)	(5)	(6)	(7)	(8)	(9)	(10)		(11)	(12)	(13)
0116+319	4C 31.04	Nucleus	01 16 47.249	31 55 05.83	< 0.06	< 0.03	-	1226±16	< 1.5	-	1144	5.1	
0134+329	3C 48	North	01 34 49.834	32 54 20.45	0.10±0.02	< 0.11	22±26	1394±108	7.0	90	1101	2.7	
		South	01 34 49.829	32 54 20.23	0.23±0.04	0.04±0.02	12±1	1360±243	11.6	-55			
0221+276	3C 67	North	02 21 18.043	27 36 39.38	0.4 ±0.2	0.11±0.03	164±2	117±71	< 26	-			
		South	02 21 18.059	27 36 37.03	0.14±0.01	0.10±0.01	4±5	270±12	< 3	-	174.8	2.0	
0429+415	3C 119	Nucleus	04 29 07.899	41 32 08.55	0.05±0.01	< 0.05	101±6	1685±18	12.6	-50	1555	3.1	Visibility ~ 82% at 10^6 λ baseline.
0518+165	3C 138	West	05 18 16.520	16 35 26.85	< 0.11	< 0.11	-	883±81	7.0	-65			
		East	05 18 16.543	16 35 26.96	0.17±0.02	0.04±0.02	63±1	1733±167	21.3	-13	1128	2.5	
0538+498	3C 147	West	05 38 43.498	49 49 42.80	< 0.07	< 0.07	-	991±32	2.1	45			
		Central	05 38 43.512	49 49 42.89	0.07±0.02	0.02±0.01	50±2	2261±38	5.4	65	2073	2.0	
		North	05 38 43.529	49 49 43.28	0.21±0.03	0.07±0.02	8±2	218±24	13.8	90			
1117-248	-	West	11 17 40.923	-24 51 41.38	< 0.09	< 0.09	-	146±15	< 12	-	132.8	5.3	
		East	11 17 40.938	-24 51 41.56	< 0.09	< 0.09	-	141±13	< 12	-			
1153+317	4C 31.38	North	11 53 44.119	31 44 46.79	< 0.10	< 0.10	-	100±9	< 11	-			
		South	11 53 44.071	31 44 46.12	< 0.07	< 0.07	-	183±10	< 6	-	162.3	3.7	
1203+645	3C 268.3	North	12 03 54.089	64 30 18.89	0.07±0.01	0.06±0.01	-	252±13	< 5	-	202.2	3.5	
		South	12 03 54.158	64 30 17.63	-	-	-	> 29	< 24	-			Gaussian model fitting divergent.
1250+568	3C 277.1	West	12 50 15.117	56 50 37.05	-	-	-	> 30	< 33	-			Gaussian model fitting divergent.
		Central	12 50 15.216	56 50 36.35	< 0.07	< 0.07	-	41±4	< 23	-			
		East	12 50 15.256	56 50 36.06	< 0.06	< 0.06	-	131±8	< 8	-	113.3	3.3	
1328+254	3C 287	Nucleus	13 28 15.930	25 24 37.51	0.06±0.01	0.03±0.01	179±1	1875±12	4.8	0	1690	2.8	Visibility ~84% at 10^6λ baseline.
1328+307	3C 286	Nucleus	13 28 49.663	30 45 58.67	< 0.05	< 0.05	-	4201±66	12.7	35	3710	3.4	Visibility ~90% at 10^6λ baseline.
1345+125	4C 12.50	Nucleus	13 45 06.168	12 32 20.40	0.04±0.01	0.02±0.01	179±5	1064±7	12	-40	1020	2.8	Visibility ~95% at 10^6λ baseline.
1419 + 419	3C 299	Nucleus	14 19 06.447	41 58 30.41	< 0.14	< 0.14	-	85±20	< 15	-	65.6	3.3	Gaussian fit to central part only.
1437+624	-	Nucleus	14 37 32.045	62 24 46.99	< 0.13	< 0.13	-	326±9	< 4	-	245.5	2.8	Visibility ~60% at 10^6λ baseline.
1442+101	OQ 172	Nucleus	14 42 50.463	10 11 11.92	< 0.03	< 0.03	-	464±5	< 2	-	455.0	2.9	
1458+718	3C 309.1	West	14 58 56.650	71 52 11.15	0.04	< 0.006	162±2	1583	3.8	45	1475	2.1	No Gaussian fits available. Size is from Kus et al. 1981. Flux densities are integrated values. Positions and polarization are at peak intensities.
		East	14 58 56.851	71 52 11.04	-	-	-	186	< 11	-			
1629+680	4C 68.18	Nucleus	16 29 50.832	68 03 38.89	0.09±0.01	0.04±0.01	169±2	212±6	< 7	-	174.6	2.5	Visibility ~80% at 10^6λ baseline.
1634+628	3C 343	Nucleus	16 34 01.080	62 51 41.83	0.05±0.01	0.04±0.01	7±4	484±5	4	55	446.1	2.6	Visibility ~80% at 10^6λ baseline.
1637+626	3C 343.1	West	16 37 55.315	62 40 34.33	< 0.10	< 0.10	-	293±21	< 3	-	257.5	2.5	
		East	16 37 55.347	62 40 34.30	< 0.09	< 0.09	-	164±7	< 6	-			
1901+319	3C 395	West	19 01 02.271	31 55 14.32	0.12±0.01	0.07±0.01	97±2	85±4	< 20	-			
		East	19 01 02.309	31 55 13.91	0.04±0.01	0.02±0.01	113±2	1899±17	5	50	1841	3.6	
2230+114	CTA 102	Nucleus	22 30 07.809	11 28 22.69	< 0.01	< 0.01	-	5353±17	3.3	45	5340	7	
2247+140	4C 14.82	North	22 47 56.712	14 03 57.38	0.07±0.01	0.04±0.01	49±2	697±19	1.2	90	620.2	2.1	
		South	22 47 56.706	14 03 57.24	< 0.10	< 0.10	-	292±17	13	20			

TABLE III. 6-cm parameters.

Source	Other Name	Component	RA(1950) H M S	DEC(1950) D M S	Major Axis (arcs)	Minor Axis (arcs)	PA (deg)	Flux Density (mJy/beam)	Polarization %	PA	Peak Total Intensity (mJy/beam)	rms Noise (mJy/beam)	Comments
(1)	(2)	(3)	(4)	(5)	(6)	(7)	(8)	(9)	(10)		(11)	(12)	(13)
0221+276	3C 67	North	02 21 18.052	27 36 39.51	0.61±0.05	0.21±0.02	174±1	337±2	Complex				
		South	02 21 18.067	27 36 37.34	0.18±0.01	0.15±0.01	173±15	561±12	< 0.2	-	470.7	0.7	
0518+165	3C 138	Nucleus	05 18 16.548	16 35 27.26	~ 0.8	< 0.1	72±2	3974±245	14.0	-12	2733	5	One component Gaussian fit not very good.
1153+317	4C 31.38	North	11 53 44.117	31 44 46.76	< 0.22	< 0.22	-	358±38	1.5	40			
		South	11 53 44.071	31 44 46.10	0.13±0.03	< 0.13	27±40	670±28	1.0	-13	588.9	1.2	
1203+645	3C 268.3	North	12 03 54.046	64 30 18.82	0.16±0.01	0.08±0.01	145±2	746±12	0.3	-28	656.8	1.1	
		South	12 03 54.113	64 30 17.56	0.4 ±0.01	< 0.35	54±8	533±136	7.3	-79			One component Gaussian fit not very good.
1250+568	3C 277.1	North	12 50 15.076	56 50 37.01	0.26±0.02	0.15±0.02	138±3	254±13	5.8	- 7			
		South	12 50 15.210	56 50 36.05	0.21±0.02	< 0.21	132±19	463±28	< 0.5	-	353.5	1.0	
1328+307	3C 286	West	13 28 49.478	30 45 57.52	0.56±0.07	0.27±0.04	47±2	68±9	24	83			
		East	13 28 49.657	30 45 58.62	0.24±0.03	< 0.23	93±15	(8600±500)	11.7	32	7236	2.6	One component Gaussian fit not very good.
1419 + 419	3C 299	West	14 19 05.479	41 58 25.25	0.42±0.05	0.24±0.04	58±3	44±6	29.7	69			
		East	14 19 06.407	41 58 30.23	0.49±0.02	0.23±0.02	16±1	839±28	< 0.5	-	431.3	0.8	
1458+718	3C 309.1	West	14 58 56.369	71 52 10.54	0.37±0.04	< 0.38	50±13	172±15	2	45			
		Central	14 58 56.595	71 52 11.14	< 0.16	< 0.16	-	2497±58	5.2	53	2270	2.0	
		East	14 58 56.776	71 52 11.06	0.45±0.06	0.24±0.04	111±2	662±82	Complex				
1901+319	3C 395	West	19 01 02.270	31 55 14.29	0.53±0.10	< 0.51	11±9	221±49	9.6	10			
		East	19 01 02.309	31 55 13.91	< 0.11	< 0.11	-	1284±16	7.5	70	1252	1.1	

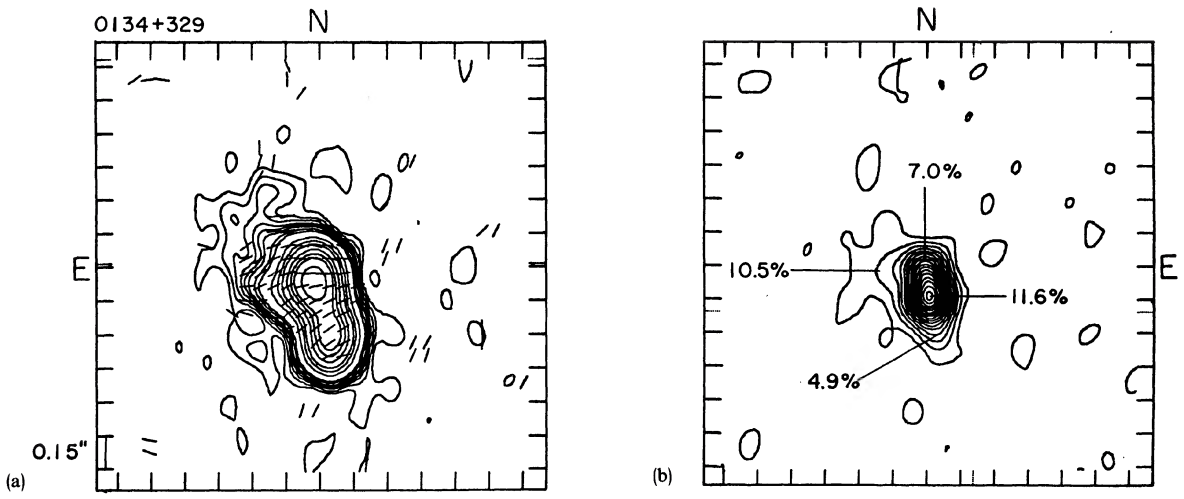

FIGS. 1–14. VLA maps at λ 2 cm with $0.15'' \times 0.15''$ resolution of SSC's with extended radio emission: (a) total intensity with polarization position angles superimposed, the length scales of the bars are arbitrary; (b) polarized intensity. The contour values are given in Table IV. Negative values, if present, are represented by dashed contours. The percentages polarization in selected regions is also indicated in the figures.

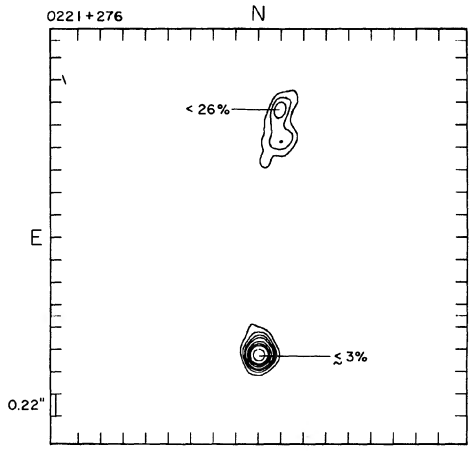

FIG. 2.

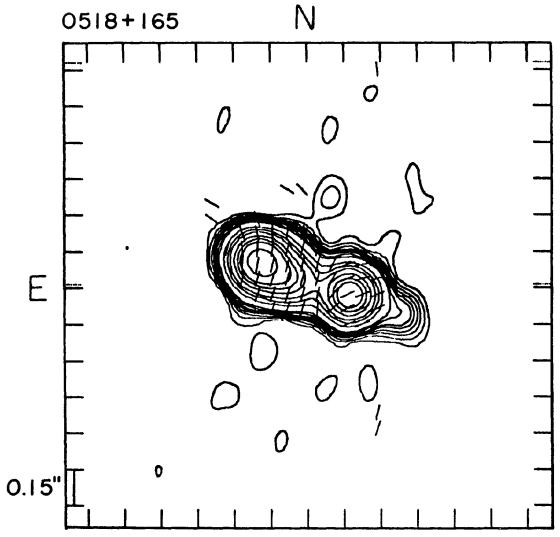

FIG. 3(a)

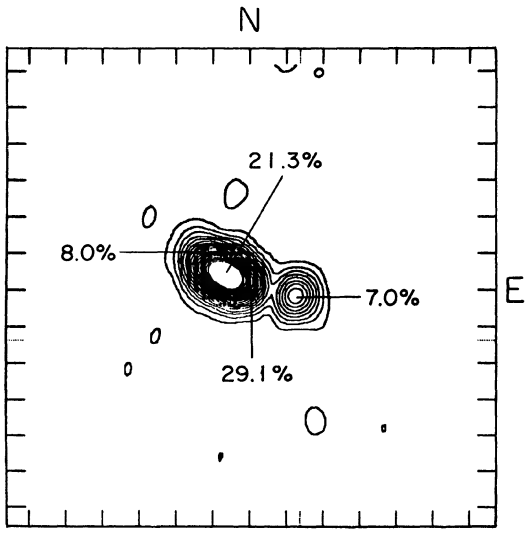

FIG. 3(b)

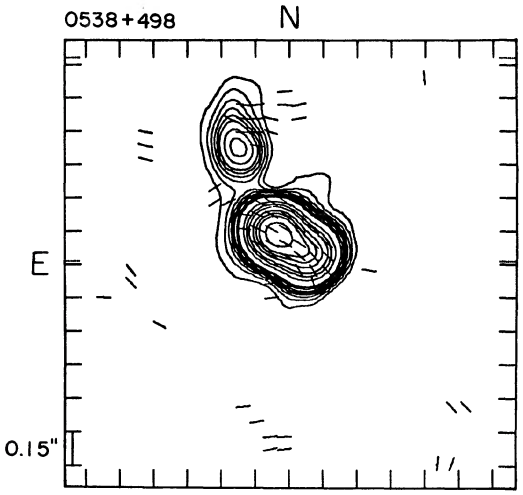

FIG. 4(a)

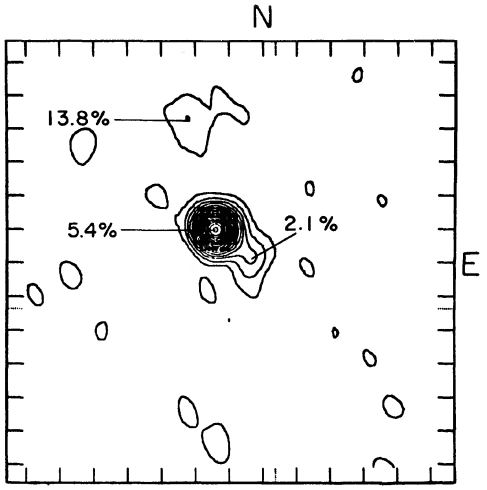

FIG. 4(b)

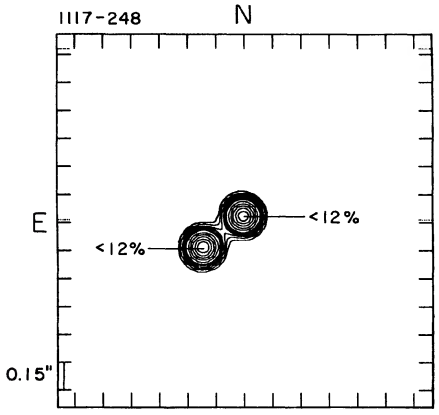

FIG. 5.

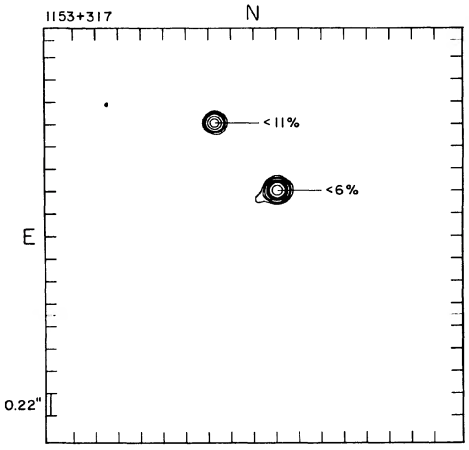

FIG. 6.

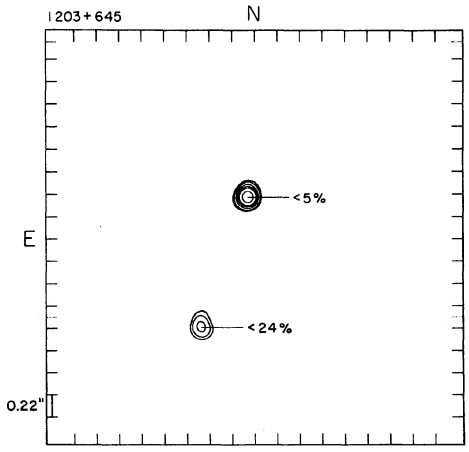

FIG. 7.

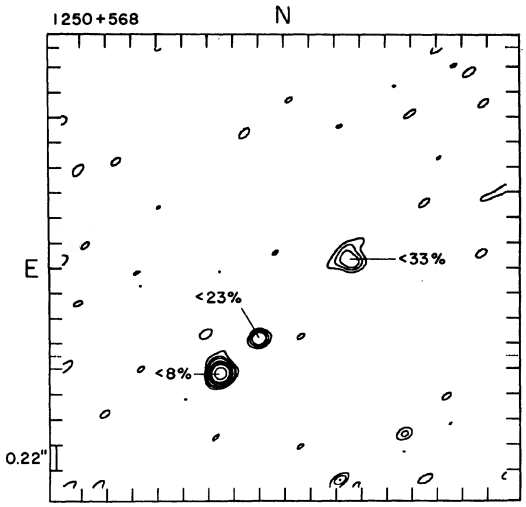

FIG. 8.

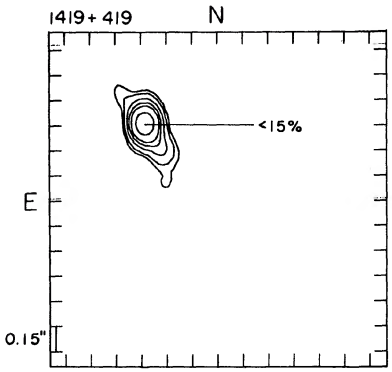

FIG. 9.

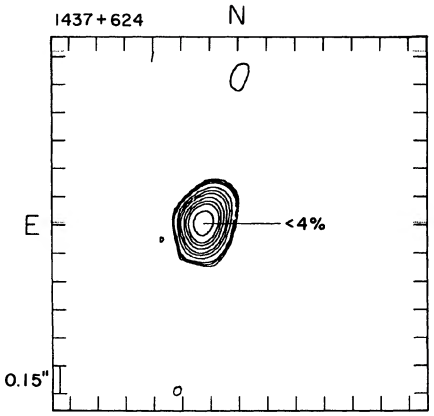

FIG. 10.

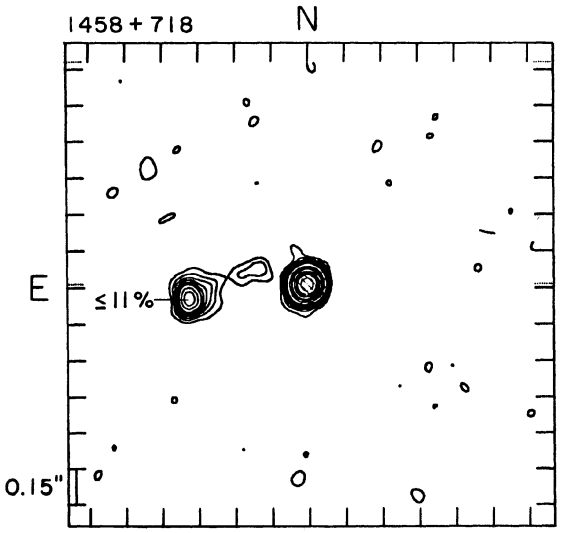

FIG. 11(a)

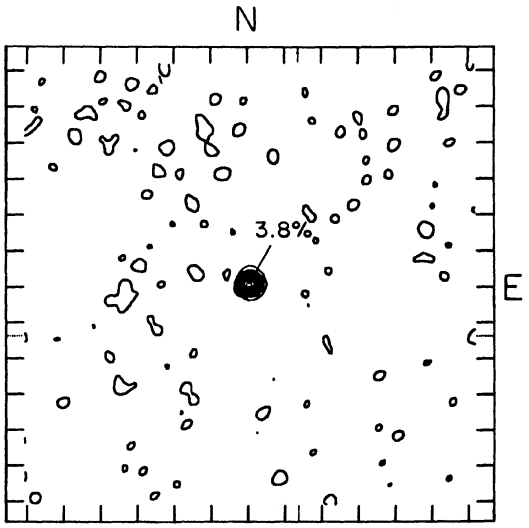

FIG. 11(b)

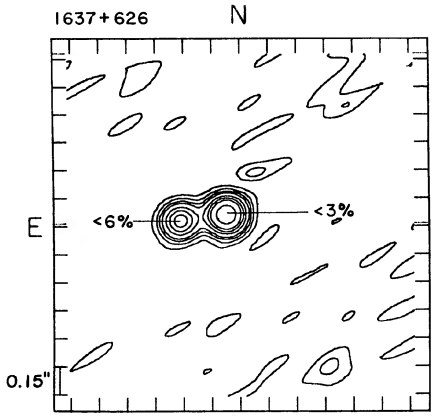

FIG. 12.

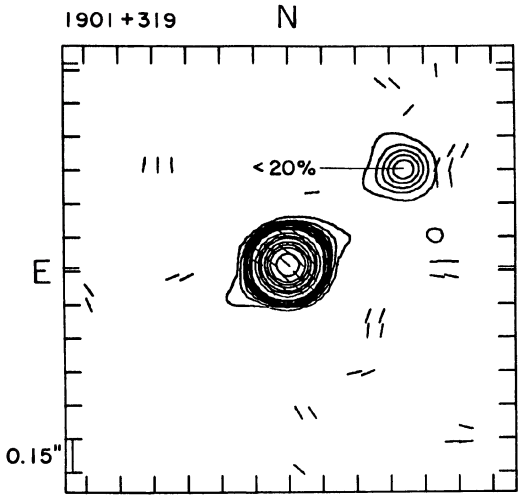

FIG. 13(a)

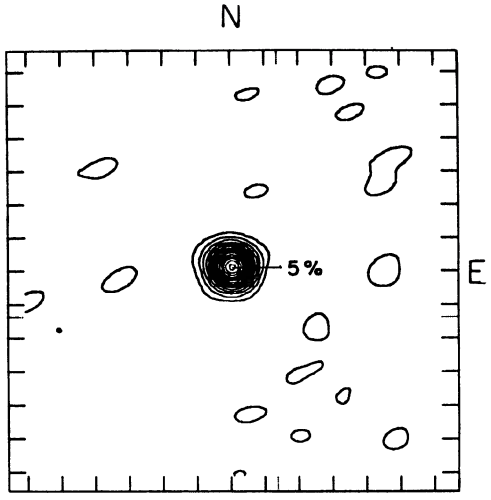

FIG. 13(b)

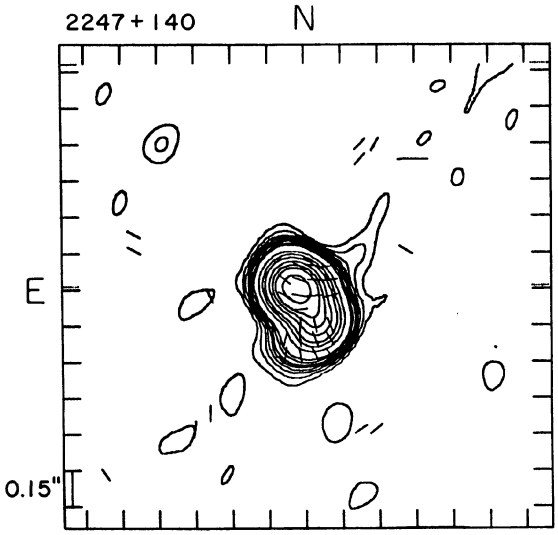

FIG. 14(a)

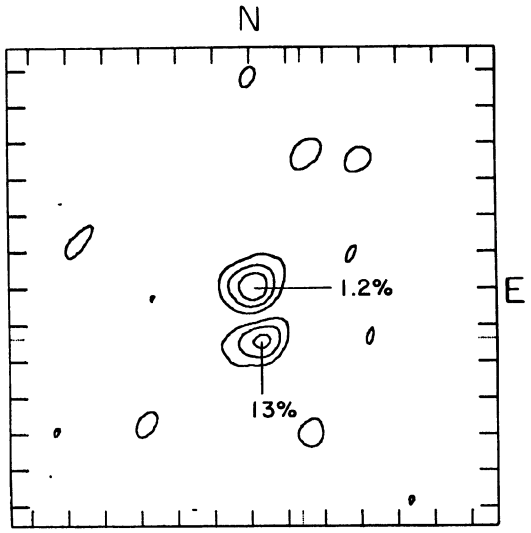

FIG. 14(b)

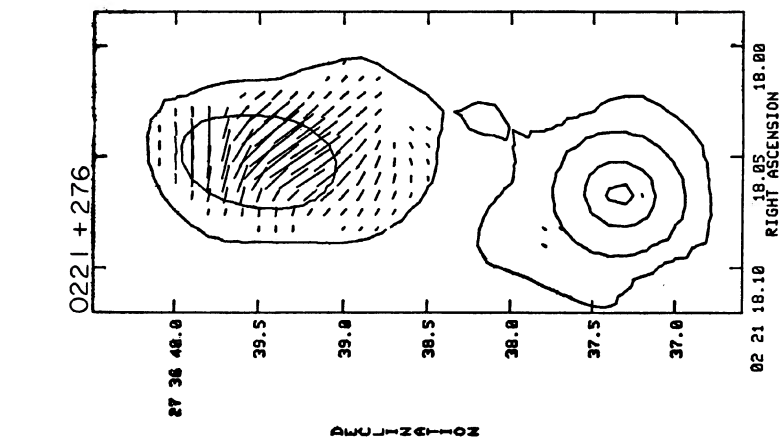

FIG. 15(c).

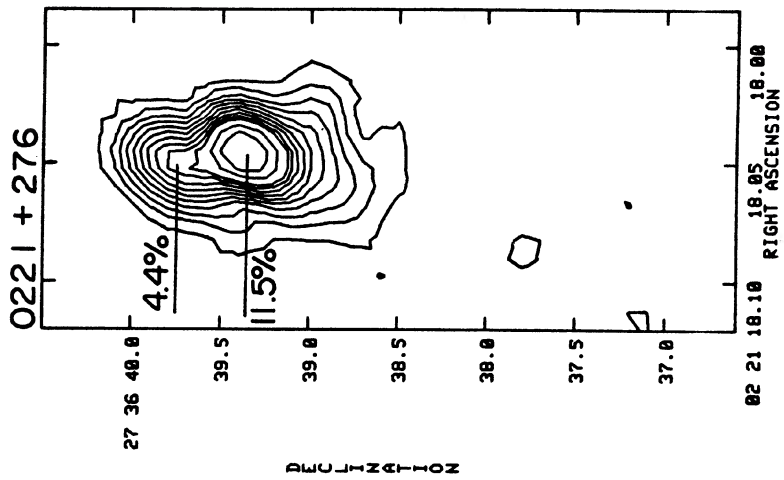

FIG. 15(b).

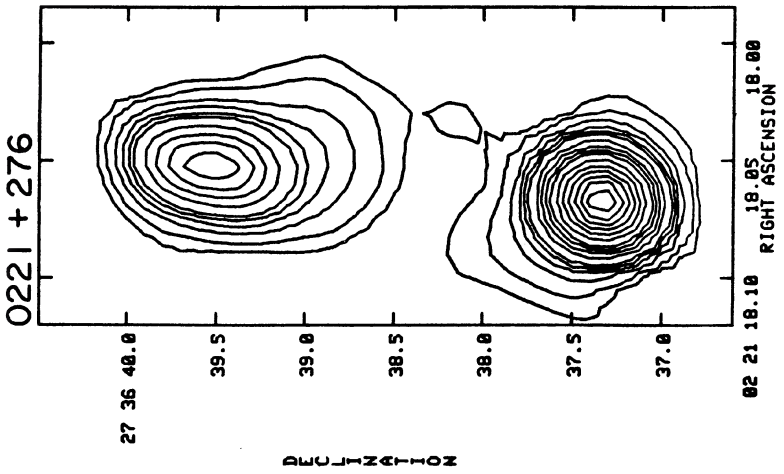

FIG. 15(a).

FIGS. 15–23. VLA maps at λ 6 cm with 0.4" $\times$ 0.4" resolution of some large SSC's: (a) total intensity; (b) polarized intensity; (c) polarization position angles superimposed on total intensity contours. The contour values and length scales are given in Table V. Negative values, if present, are represented by dashed contours. The percentages polarization in selected regions are also indicated in the figures.

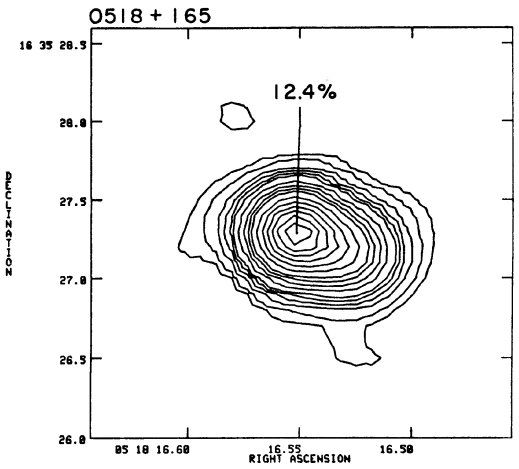

FIG. 16(a)

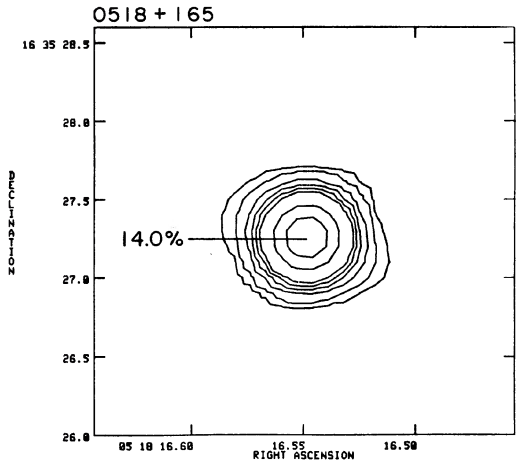

FIG. 16(b)

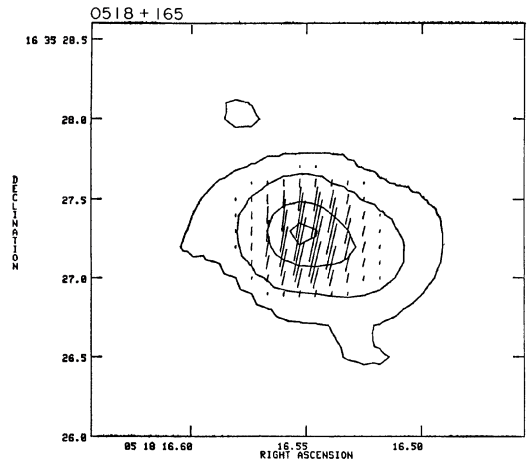

FIG. 16(c)

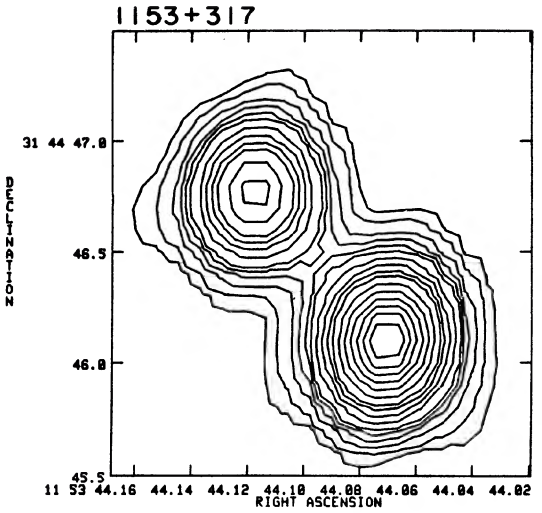

FIG. 17(a)

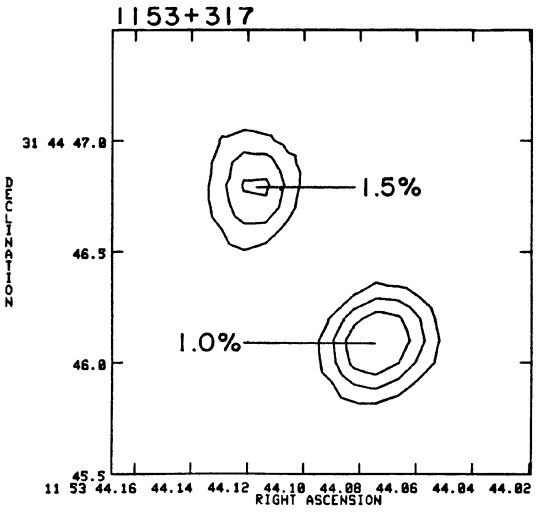

FIG. 17(b)

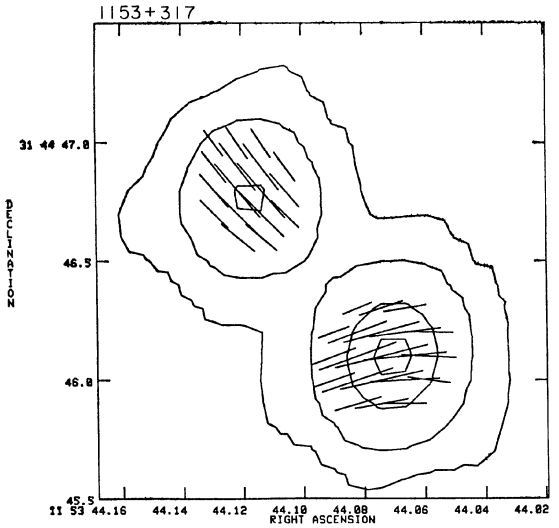

FIG. 17(c)

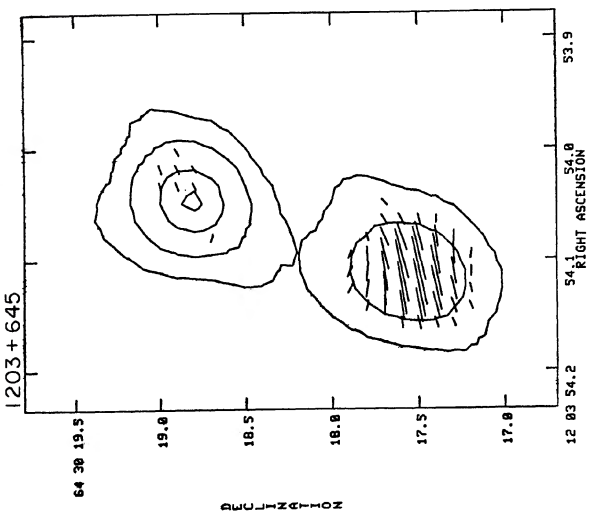

FIG. 18(c)

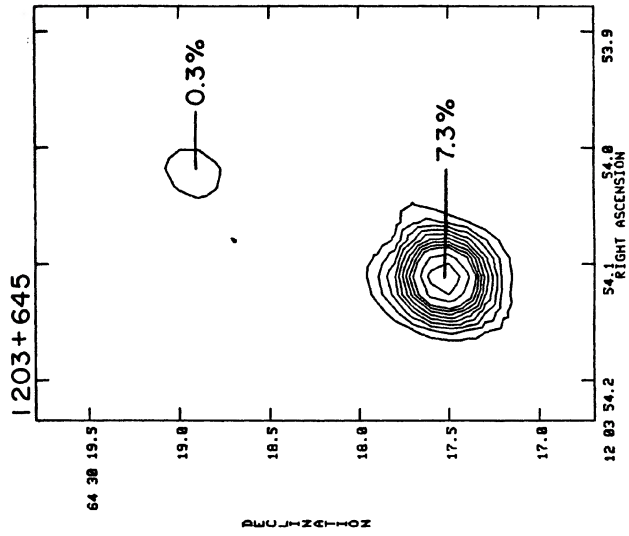

FIG. 18(b)

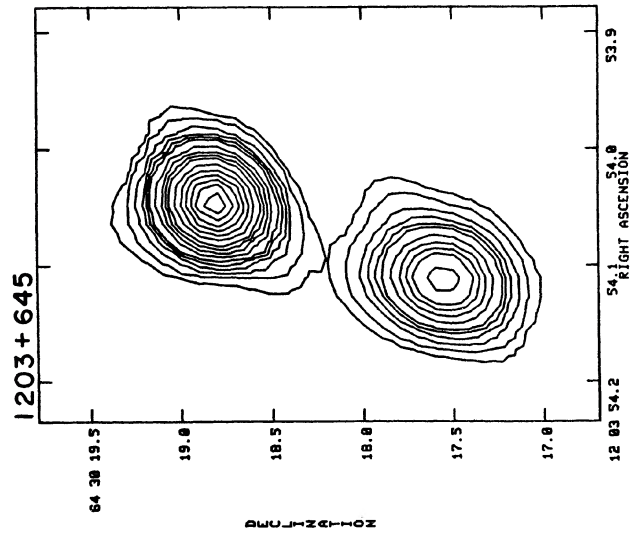

FIG. 18(a)

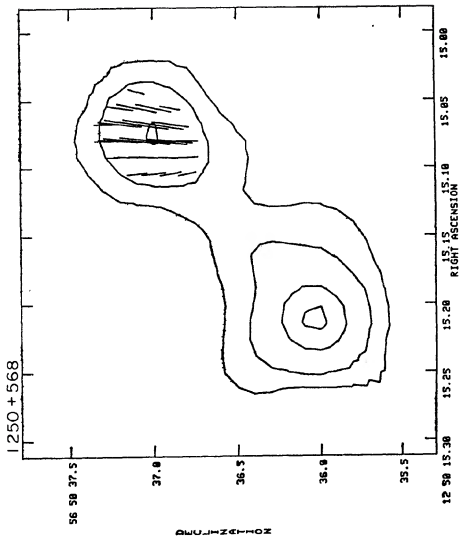

FIG. 19(c)

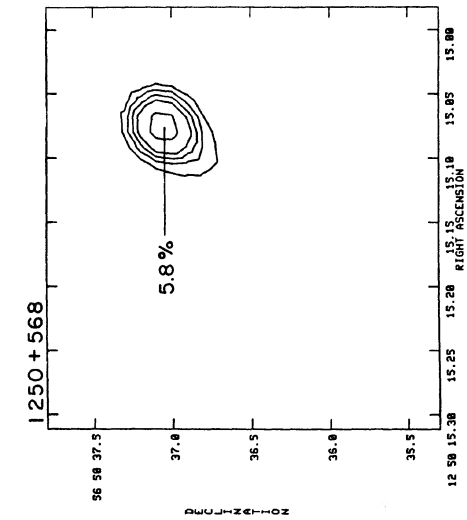

FIG. 19(b)

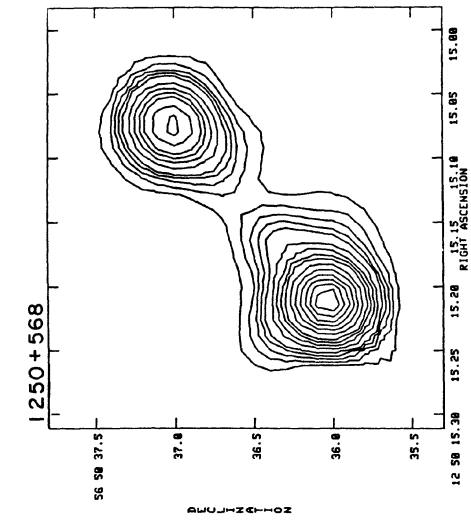

FIG. 19(a)

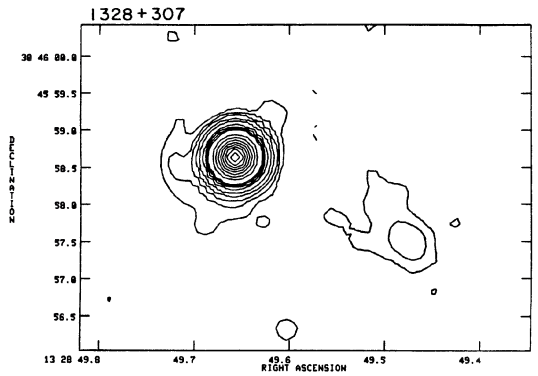

FIG. 20(a)

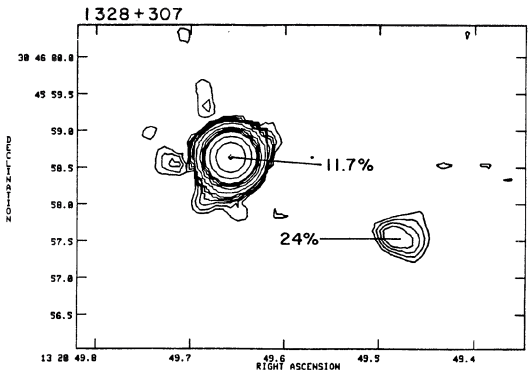

FIG. 20(b)

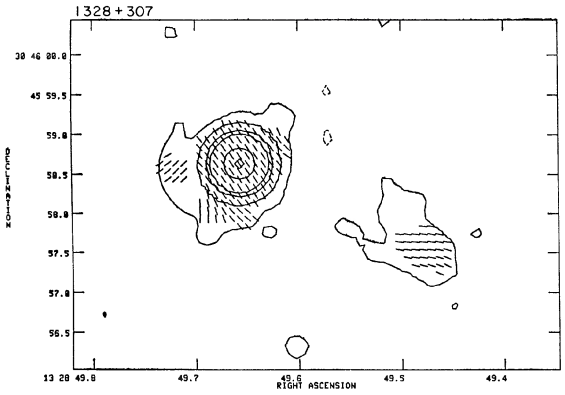

FIG. 20(c)

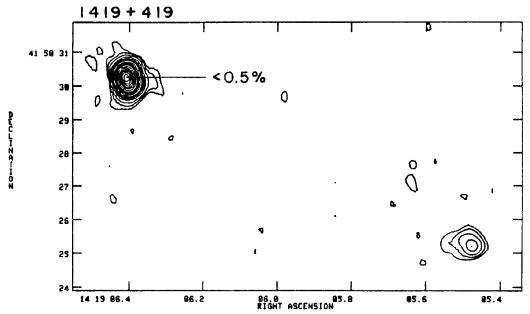

FIG. 21(a)

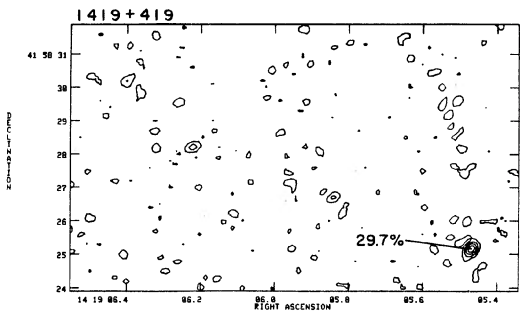

FIG. 21(b)

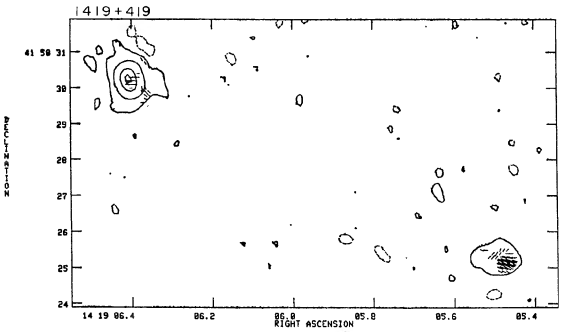

FIG. 21(c)

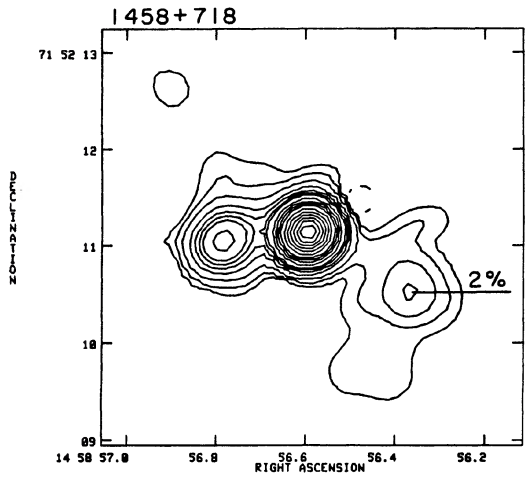

FIG. 22(a)

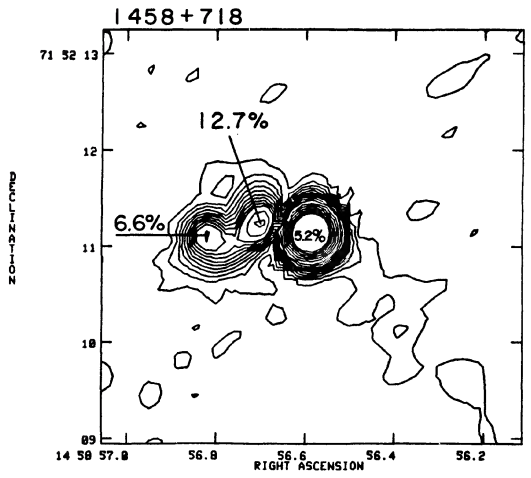

FIG. 22(b)

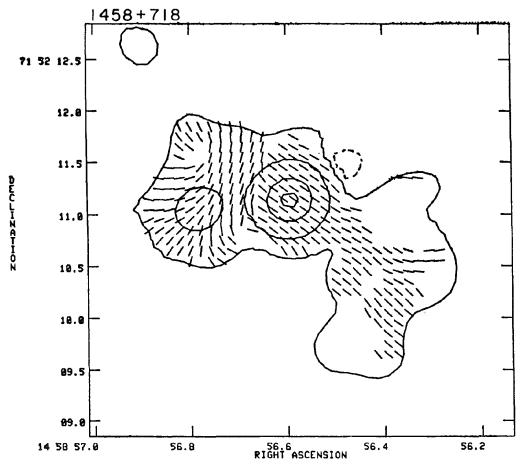

FIG. 22(c)

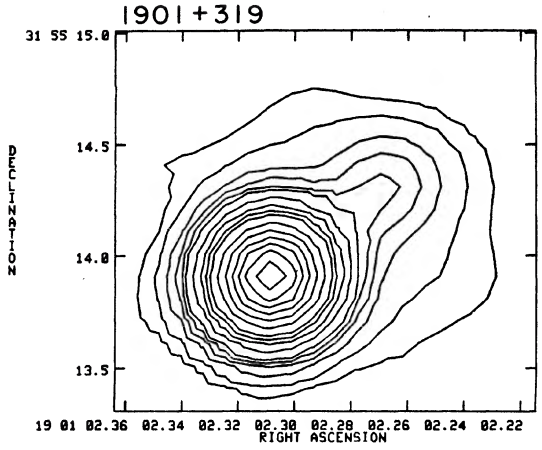

FIG. 23(a)

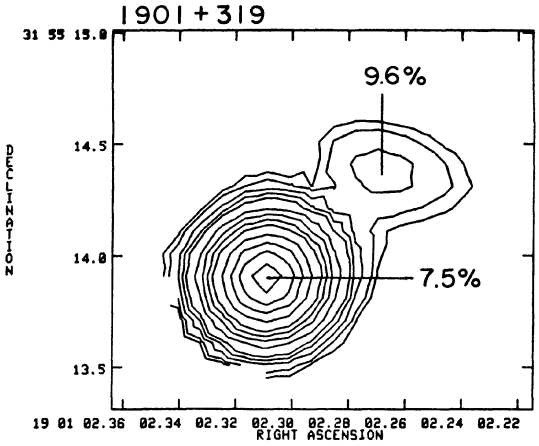

FIG. 23(b)

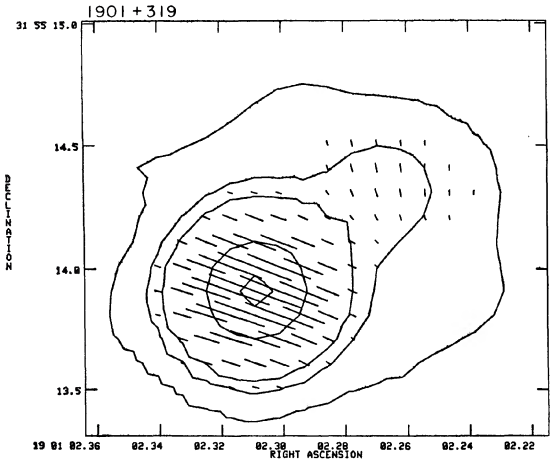

FIG. 23(c)

TABLE IV. Contour levels of 2-cm maps.

Source	Other Name	Figure Numbers	2 cm Contour levels of total intensity (I) and polarized intensity (P). Values are in mJy/beam	
0134+329	3C 48	1a	I	-5.5, 5.5, 11, 16.5, 22, 27.5, 33, 44, 55, 110, 165, 220, 330, 440, 550, 826
		1b	P	From 6 to 102 in steps of 6.
0221+276	3C 67	2	I	-8.7, 8.7, 17.5, 26.1, 35, 52.5, 70, 87.4, 131, 175
0518+165	3C 138	3a	I	-5.6, 5.6, 11.3, 16.9, 22.6, 28.2, 34, 45, 56.4, 113, 169, 226, 338.5, 451, 564, 846
		3b	P	From 6 to 120 in steps of 6.
0538+498	3C 147	4a	I	-10.4, 10.4, 20.7, 31, 41.5, 51.8, 62, 83, 104, 207, 311, 415, 622, 829, 1036, 1555
		4b	P	From 6 to 108 in steps of 6.
1117-248	--	5	I	-20, 20, 26.5, 33, 40, 46.5, 53, 66.5, 80, 93, 106, 120
1153+317	4C 31.38	6	I	-16, 16, 24.3, 32.5, 49, 65, 81, 122
1203+645	3C 268.3	7	I	-30, 30, 40, 61, 81, 101, 152
1250+568	3C 277.1	8	I	-11, 11, 17, 23, 34, 45, 57, 85
1419+419	3C 299	9	I	-9.8, 9.8, 13, 20, 26, 33, 49
1437+624	--	10	I	-7.4, 7.4, 9.8, 12.3, 24.6, 36.8, 49, 74, 98, 123, 184
1458+718	3C 309.1	11a	I	-7.4, 7.4, 14.8, 22, 29.5, 37, 44, 59, 74, 148, 221, 295, 443, 500, 738, 1106
		11b	P	From 6 to 54 in steps of 6.
1637+626	3C 343.1	12	I	-12.9, 12.9, 25.8, 39, 52, 77, 103, 129, 193
1901+319	3C 395	13a	I	-9.2, 9.2, 18.4, 27.6, 37, 46, 55, 74, 92, 184, 276, 368, 552, 737, 921, 1381
		13b	P	From 6 to 90 in steps of 6.
2247+140	4C 14.82	14a	I	-6.2, 3.1, 6.2, 9.3, 12.4, 15.5, 18.6, 24.8, 31, 62, 93, 124, 186, 248, 310, 465
		14b	P	6, 12, 18

TABLE V. Contour levels of 6-cm maps.

Source	Other name	Figure numbers		6-cm contour levels of total intensity (I) and polarized intensity (P). Values are in mJy/beam times a factor as indicated between the brackets. The length-scales of the bars representing the polarization position angles (ϕ) are in mJy/beam of polarized intensity per one arcsecond.	Peak flux density in mJy/beam
0221 + 276	3 C 67	15a	I	4.7×(−1, 1, 2, 4, 6, 8, 10, 15, 20, 25, 30, 40, 50, 60, 70, 80, 90)	470.7
		15b	P	0.3×(2, 4, 6, 8, 10, 12, 14, 16, 18, 20, 25, 30, 40, 50, 60, 70, 80, 90)	11.3
		15c	$I;\phi$	4.7×(−1, 1, 10, 50, 90); 28.3	470.7
0518 + 165	3C 138	16a	I	27.3×[as in Fig. 15(a)]	2733.0
		16b	P	0.9×(10, 20, 40, 60, 80, 100, 200, 300)	352.6
		16c	$I;\phi$	27.3×[as in Fig. 15(a)]; 881.5	2733.0
1153 + 317	4C 31.38	17a	I	5.9×[as in Fig. 15(a)]	588.9
		17b	P	0.6×(3, 5, 7)	5.8
		17c	$I;\phi$	5.9×[as in Fig. 15(a)]; 14.6	588.9
1203 + 645	3C 268.3	18a	I	6.6×[as in Fig. 15(a)]	656.8
		18b	P	0.6×(4, 6, 8, 10, 12, 14, 16, 18, 20, 25, 30)	21.2
		18c	$I;\phi$	6.6×[as in Fig. 15(a)]; 52.9	656.8
1250 + 568	3C 277.1	19a	I	3.5×(−2, 2, 4, 6, 8, 10, 15, 20, 25, 30, 40, 50, 60, 70, 80, 90)	353.5
		19b	P	0.6×(4, 6, 8, 10, 15)	10.3
		19c	$I;\phi$	3.5×(−2, 2, 10, 50, 90)	353.5
1328 + 307	3C 286	20a	I	72.4×(−0.1, 0.1, 0.25, 0.5, 1, 2, 4, 6, 8, 10, 20, 30, 40, 50, 60, 70, 80, 90)	7236.0
		20b	P	1.0×(3, 4, 5, 6, 8, 10, 20, 40, 60, 80, 100, 200, 400, 800)	343.8
		20c	$I;\phi$	72.4×(−0.1, 0.1, 1, 5, 10, 50, 90); arbitrary length scale	7236.0
1419 + 415	3C 299	21a	I	4.3×(−1, 0.5, 1, 2, 4, 6, 8, 10, 15, 20, 25, 30, 40, 50, 60, 70, 80, 90)	431.3
		21b	P	0.7×(2, 4, 6, 8)	7.0
		21c	$I;\phi$	4.3×(−0.5, 0.5, 10, 50, 90); 17.5	431.3
1458 + 718	3C 309.1	22a	I	22.7×(−0.5, 0.5, 1, 2, 4, 6, 8, 10, 15, 20, 30, 40, 50, 60, 70, 80, 90)	2270.0
		22b	P	0.7×(2, 4, 6, 8, 10, 12, 14, 16, 18, 20, 25, 30, 40, 50, 60, 70, 80, 90)	110.2
		22c	$I;\phi$	22.7×(−0.5, 0.5, 10, 50, 90); arbitrary length scale	2270.0
1901 + 319	3C 395	23a	I	12.5×[as in Fig. 15(a)]	1252.0
		23b	P	1.2×(3, 4, 6, 8, 10, 15, 20, 25, 30, 40, 50, 60, 70)	93.4
		23c	$I;\phi$	12.5×(−1, 1, 5, 10, 50, 90)	1252.0

10. Percentage polarization and position angle at the peak intensity of each component. The uncertainties are $<0.5\%$ and $<5°$, respectively.

11. Peak total intensity.

12. rms noise confusion in the map.

13. Comments.

Contour maps of the extended sources are shown in Figs. 1–14 (λ 2 cm) and 15–23 (λ 6 cm). Contour levels for the λ 2 cm maps are given in Table IV and for the λ 6 cm maps in Table V.

Comments on selected individual sources are given below. For those components which were isolated and marginally resolved, we have included some spectral information (using our and Perley's λ 6 cm data).

Comments on Individual Sources

0116+319 (4C 31.04). PW find a spectral index $\alpha_{11}^{6} = 0.58$, differing with Perley 1982 ($\alpha_{21}^{6} = 0.43$) and Kuhr *et al.* 1981 ($\alpha = 0.45$ in the frequency range 318 MHz–31.4 GHz). We find that $\alpha_{6}^{2} \simeq 0.17$ and that the source may be variable at λ 2 cm, since Pauliny-Toth *et al.* (1972) have observed 1030 ± 50 mJy at 10695 MHz, while we measure 1226 ± 16 mJy at 14965 MHz.

0221+276 (3C 67). The southern component has $\alpha_{6}^{2} \simeq 0.65$.

0429+419 (3C 119). This source is barely resolved: ~0.05″ at position angle 101°. Other high-resolution observations also show structure. Donaldson *et al.* (1971) find that the source may be a double with <0.08″ separation at position angle 150°. Pearson *et al.* (1980), however, can not fit such a simple double source to their VLBI data. Instead they find a very asymmetric double with ~0.02″ separation at position angle 55° and that probably ~50% of the flux density at 1.67 GHz is on a scale of ~0.1″. Taken together, these and our data suggest a rather complex morphology for 3C 119. We find $\alpha_{6}^{2} \simeq 0.70$ and that the percentage polarization increases rapidly with decreasing wavelength: $<0.5\%$ (λ 2 cm), 0.7% (λ 6 cm), and 12.6% (λ 2 cm). The λ 20 cm and λ 6 cm data are from Perley (1982).

0538+498 (3C 147). VLBI observations by Simon *et al.* (1980) show that the southern component consists of a bright compact core and a (two-component?) jet at position angle of −127°. Higher-resolution (~0.001″) observations by Preuss *et al.* (1982) show additional structure in the nucleus, including some emission apparently at right angles to the jet. Perhaps the northwest protrusion seen at very low levels in our λ 2 cm map is related to this. We have used a two-component Gaussian model fit for the southern component and find an extended central component at position angle + 50° and a compact component (knot at the end of the jet?) along the same direction, in agreement with the VLBI observations.

1153+317 (4C 31.38). Both components appear to have a steep spectrum: $\alpha_{6}^{2} \simeq 0.97$.

1250+568 (3C 277.1). The triple structure of this source at λ 2 cm shows why Pooley and Henbest (1974) could not model their visibility data with a single or double Gaussian distribution of emission. At λ 6 cm there is evidence for additional structure to the northeast of the southern component.

1328+254 (3C 287). The percentage polarizations at λ 2 cm and λ 6 cm are comparable: 4.8% and 4.6% (Perley 1982), respectively.

1328+307 (3C 286). Our λ 6 cm map shows evidence for a component (halo?) to the east, in addition to a component to the southwest in agreement with Perley (1982). Simon *et al.* (1980) and Pearson *et al.* (1980) find that 3C 286 has a small core and jet of 0.08″ extent at position angle 225°, pointing approximately in the same direction as the southwestern

component at a position angle of 243°. The percentage polarization of the core is comparable at short wavelengths: 12.7% (λ 2 cm) and 11.7% (λ 6 cm).

1345+125 (4C 12.50). The percentage polarization increases rapidly at short wavelengths: $<0.5\%$ (λ 6 cm; Perley 1982) and 12% (λ 2 cm). PW report a spectral index $\alpha_{11}^{6} \simeq 0.51$, Perley finds $\alpha_{21}^{6} \simeq 0.49$ and Kuhr *et al.* (1981) $\alpha = 0.41$ in the 0.4 GHz–10 GHz range with a steepening spectrum $\geqslant$10 GHz. Our result of $\alpha_{6}^{2} = 0.90$ is consistent with this.

1419+415 (3C 299). Our maps confirm the secondary structure to the southwest and the resolved core as found by Laing (1981).

1437+624. We derive a spectral index $\alpha_{6}^{2} \simeq 0.88$.

1442+101 (OQ 172). Marscher and Schaffer (1980) find structure on a scale of $\sim$0.01″. The spectral index is $\alpha_{6}^{2} \simeq 0.86$.

1458+718 (3C 309.1). Our λ 6 cm map confirms the triple structure observed by Kus *et al.* (1981), Laing (1981), and Wilkinson (1982). There is also some evidence for extended emission to the north of the eastern component so that the overall structure might be *S* shaped, in agreement with the hybrid maps of Kus *et al.* and Wilkinson. Our λ 2 cm map shows that the eastern component contains a jet which is misaligned with the nucleus. The spectrum of the central component is relatively flat: $\alpha_{6}^{2} \simeq 0.41$. The percentage polarization of short wavelengths is comparable: 5.2% (λ 6 cm) and 3.8% (λ 2 cm).

1634+628 (3C 343). The polarization peaks $\sim$0.03″–0.06″ east of the nucleus. The spectral index $\alpha_{6}^{2} \simeq 1.0$. The percentage polarization may increase rapidly at short wavelengths: $\sim$1.1% (λ 6 cm, Perley 1982), 4% (λ 2 cm).

1901+319 (3C 395). VLBI observations by Phillips and Mutel (1980) show that the southern component is a double with 0.016″ separation at a position angle of $-$ 62°, which is close to that of the secondary observed at λ 2 cm at 0.7″ and position angle $-$ 53°. Our observations show further that the southern component has an inverted spectrum ($\alpha_{6}^{2} \simeq -0.35$) and is variable at both wavelengths (by comparing with the spectrum given in Fig. 3 of Phillips and Mutel). This source might therefore belong to the class of objects which exhibit fast expansion and further VLBI monitoring would be useful.

2230+114 (CTA 102). This source is a well-known variable (see, for example, Balonek 1982) and its spectrum is complex (Kuhr *et al.* 1981; Balonek 1982). Peacock and Wall (1982) find $\alpha_{11}^{6} \simeq 0.50$, while Perley (1982) finds $\alpha_{21}^{6} \simeq 0.34$. This disagreement is probably due to the source's variability. Note for example that Laing (1981) observes a flux density at λ 2 cm of 2.52 $\pm$ 0.13 Jy on 10 November 1976 and that we measure 5.35 $\pm$ 0.02 Jy on 27 February 1982. We have not detected the secondary (at λ 2 cm) reported by Perley (1982) at 1.6″ from the nucleus at position angle 140°. Pearson *et al.* (1980) report structure on a scale of $\sim$0.015″ at a similar position angle of 146°.

IV. DISCUSSION

On the basis of their spectral indices in the 1 GHz–15 GHz range three objects in our sample should not be classified as SSC's: 0116 + 319, (4C 31.04), 1901 + 319 (3C 395), and 2230 + 114 (CTA 102). The last two sources are variable.

Except for 1442 + 101 (OQ 172), the most distant object in the sample, all SSC's have structure on a scale larger than 0.05″. The total linear sizes range from 0.1 kpc to 24 kpc, the largest ($>$10 kpc) objects being 1329 + 307 (3C 286), 1419 + 415 (3C 299), and 1458 + 718 (3C 309.1).

While the resolution of our maps is only sufficient to show the "large scale" structures of the SCC's, they suggest complex morphologies for the most extended objects which are rather similar to those of nearby SSC's. VLBI and MERLIN observations of several of the sources in our sample show likewise complex morphologies (Dr. Carla Fanti, private communication, 1983) which appear not grossly different for galaxies and quasars (Fanti *et al.* 1983).

The three largest objects mentioned above all have a steep spectrum radio core whose orientation is misaligned with the axis defined by the larger scale radio emission ("lobes"). The similarity to 3C 293 (Bridle *et al.* 1982; van Breugel *et al.* 1983a) is striking.

In general the (integrated) percentage polarization of SSC's at λ 6 cm is much lower than that of large ($>$100-kpc-size) steep-spectrum source components and of small ($<$1-pc-size) flat-spectrum source components. Using the single dish polarization measurements catalogued by Tabara and Inoue (1980) we find that approximately 27% of *all* sources have $<2\%$ polarization at λ 6 cm. This compares with $\sim$70% for the unresolved steep-spectrum sources in PW's list (after excluding the flat-spectrum sources mentioned in Sec. I) and $\sim$80% of such sources in Perley's sample. Approximately 50% of the compact flat-spectrum sources in the latter sample also exhibit $<2\%$ polarization at λ 6 cm.

Of the SSC's we observed with the VLA, $\sim$60% have $<2\%$ polarization at λ 6 cm. Several objects seem to become more "Faraday transparent" at shorter wavelengths: 50% of the sources have a comparable or larger percentage polarization at λ 2 cm (Table II).

The large fraction of SSC's with little polarized emission at λ 6 cm, and the trend that they become more Faraday transparent at shorter wavelengths, suggests that these objects contain relatively dense ionized gas (presumably in the associated NLR's) which depolarizes the radio emission through the effects of Faraday dispersion (Burn 1966).

The radio luminosities of the SSC's in our sample are large, ranging from 10^{25} to 10^{29} W Hz^{-1} at 1.4 GHz (Table I). Combining that with our observed sizes and using the assumption-ridden minimum energy arguments (e.g., Miley 1980) results in pressures ranging from 10^{9} to $>6\times10^{10}$ K cm^{-3}. For typical NLR parameters ($T\sim10^{4}$ K, $n_e \sim 10^{3}$–10^{4} cm^{-3}) these pressures may significantly exceed those of the line emitting gas, providing further evidence for interaction between the SSC's and a dense NLR-associated medium (see, for example, 3C 305, Heckman *et al.* 1981; 3C 293, van Breugel *et al.* 1983a).

The spectra of many SSC's flatten or turn over at frequencies less than a few hundred MHz (PW). Examples are, in order of radio luminosity: NGC 1068, 3C 293, and 3C 286 (see Kuhr *et al.* 1981). The usual interpretation of spectral "bumps" is that these are due to synchrotron self-absorption in very compact (parsec-sized) radio source components. We wish to emphasize, however, that the *low* frequency turnovers in SSC's may quite naturally be explained by free-free absorption of the radio emission by clouds in the associated NLR's.

The importance of thermal free-free absorption and emission in Seyfert galaxies in relatively *high* frequencies (5 GHz) has recently been investigated by Ulvestad *et al.* (1981), who conclude that free-free absorption might occur in the parsec-

sized broad line regions (BLR's) and free-free emission in the kiloparsec-sized NLR's.

At much *lower* frequencies, however, free-free absorption becomes important in the NLR's. For typical cloud parameters in Seyfert NLR's (thermal electron density 10^3–10^4 cm^{-3}, temperature 10^4 K, cloud-filling factor 10^{-4} and a line of sight through the source of a few hundred parsec) one can show that free-free absorption will cause a spectral turnover at frequencies less than a few hundred MHz if the clouds cover a large fraction of the source [see, for example, De Bruyn 1976; Pedlar *et al.* 1983 (NGC 1068); Charlesworth and Spencer 1982 (M87); van Breugel 1983; Pedlar *et al.* 1983 (Mk 3).

The detection of radio recombination lines in the Seyfert galaxy Mk 668 (OQ 208) also supports such an interpretation (Bell and Seaquist 1980). Also, free-free absorption could simply explain the low-frequency variability in certain compact radio sources, thus avoiding the inferred ultrahigh brightness temperatures (10^{15} K) and so-called "Compton catastrophe" in these objects (Marscher 1979).

V. CONCLUSIONS

The radio properties of distance and powerful SSC's resemble those of nearby, weaker objects such as Seyferts and sources like 3C 293, 3C 305, M87, and 4C 26.42. Also, optically there may be similarities and it appears quite general that SSC's are embedded in dense, gaseous environments.

The qualitative picture that combines all the radio and optical features of SSC's in a natural way is that they are due to jets propagating through dense and inhomogeneous interstellar media. These jets collide with clouds and presumably entrain (heat and accelerate) the ambient gas. This may account for the bright radio emission (shocks in the jets), optical associated NLR's [through local (?) photo-and/or shock ionization of clouds], the wide emission lines (accelerated clouds), the depolarization (entrained clumpy gas), the steep-spectrum turnovers (free-free absorption by the ionized clouds), and the distorted morphologies (bending of the jets by rotating gaseous disks or collisions with massive clouds).

Because of these many related properties SSC's are very important for our understanding of how extragalactic jets interact with their environment. To put the above ideas on a firmer statistical basis further detailed studies of such objects seem warranted.

It is a pleasure to thank the NRAO staff at the VLA, and in particular Peggy Perley, for their excellent service and the pleasant atmosphere. W. v. B. acknowledges partial support by ZWO (The Netherlands Organization for Pure Research) during a visit to Leiden Observatory, where part of this work was carried out.

REFERENCES

Balonek, T. J. (1982). Ph.D. thesis.
Bell, M. B., and Seaquist, E. R. (1980). Astrophys. J. **238**, 818.
Boroson, T. A., and Oke, J. B. (1982). Nature **296**, 397.
Bridle, A. H., and Fomalont, E. B. (1978). Astron. J. **83**, 704.
Bridle, A. H., Fomalont, E. B., and Cornwell, T. J. (1981). Astron. J. **86**, 1294.
Burbidge, G., and Crowne, A. H. (1979). Astrophys. J. Suppl. **40**, 583.
Burn, B. J. (1966). Mon. Not. R. Astron. Soc. **133**, 67.
Charlesworth, M., and Spencer, R. E. (1982). Mon. Not. R. Astron. Soc. **200**, 933.
de Bruyn, A. G. (1976). Astron. Astrophys. **52**, 439.
de Bruyn, A. G., and Wilson, A. S. (1978). Astron. Astrophys. **64**, 433.
De Young, D. S., Condon, J. J., and Butcher, H. R. (1980). Astrophys. J. **242**, 511.
Donaldson, W., Miley, G. K., and Palmer, H. P. (1971). Mon. Not. R. Astron. Soc. **152**, 145.
Fanti, C. (1983). Private communication.
Fanti, C., Fanti, R., Parma, P., and Schilizzi, R. T. (1983). To be published in *Proceedings of IAU Symposium No. 110.*
Ford, H. C., and Butcher, H. (1979). Astrophys. J. Suppl. **41**, 147.
Heckman, T. M., Miley, G. K., van Breugel, W. J. M., and Butcher, H. (1981). Astrophys. J. **247**, 403.
Heckman, T. M., Miley, G. K., Balick, B., van Breugel, W. J. M., and Butcher, H. (1982). Astrophys. J. **262**, 529.
Heckman, T. M., Balick, B., van Breugel, W. J. M., and Miley, G. K. (1983). Astron J. **88**, 583.
Hewitt, A., and Burbidge, G. (1980). Astrophys. J. Suppl. **43**, 57.
Hutchings, J. B., and Campbell, G. (1983). Preprint.
Kuhr, H., Witzel, A., Pauliny-Toth, I. I. K., and Nauber, U. (1981). Astron. Astrophys. Suppl. **45**, 367.
Kus, A. J., Wilkinson, P. N., and Booth, R. S. (1981). Mon. Not. R. Astron. Soc. **194**, 527.
Laing, R. A. (1981). Mon. Not. R. Astron. Soc. **194**, 301.
Marscher, A. P. (1979). Astrophys. J. **228**, 27.
Marscher, A. P., and Shaffer, D. B. (1980). Astron. J. **85**, 668.
Miley, G. K. (1980). Annu. Rev. Astron. Astrophys. **18**, 165.
Pauliny-Toth, I. I. K., Kellermann, K. I., Davis, M. M., Fomalont, E. B., and Shaffer, D. B. (1972). Astron. J. **77**, 265.
Peacock, J. A., and Wall, J. V. (1982). Mon. Not. R. Astron. Soc. **198**, 843 (PW).
Pearson, T. J., Readhead, A. C. S., and Wilkinson, P. N. (1980). Astrophys. J. **236**, 714.
Pedlar, A., Booler, R. V., Spencer, R. E., and Steward, O. J. (1983). Mon. Not. R. Astron. Soc. **202**, 647.
Pedlar, A., Unger, S. W., and Booler, R. V. (1983). Mon. Not. R. Astron. Soc. (in press).
Perley, R. A. (1982). Astron. J. **87**, 859.
Phillips, R. B., and Mutel, R. L. (1980). Astrophys. J. **236**, 89.
Pooley, G. G., and Henbest, S. M. (1974). Mon. Not. R. Astron. Soc. **169**, 477.
Preuss, E., Alef, W., Pauliny-Toth, I. I. K., and Kellermann, K. I. (1982). In *Proceedings of IAU Symposium No. 97,* edited by D. S. Heeschen and C. M. Wade (Reidel, Dordrecht), p. 289.
Schilizzi, R. T., Miley, G. K., Janssen, F. L. J., Wilkinson, P. N., Cornwell, T. J., and Fomalont, E. B. (1981). Report No. ESA SP-162, p. 107.
Simon, R. S., Readhead, A. C. S., Moffet, A. T., Wilkinson, P. N., and Anderson, B. (1980). Astrophys. J. **236**, 707.
Tabara, H., and Inoune, M. (1980). Astron. Astrophys. Suppl. **39**, 379.
Thompson, A. R., Clark, B. G., Wade, C. M., and Napier, P. J. (1980). Astrophys. Suppl. **44**, 151.
Ulvestad, J. S., Wilson, A. S., and Sramek, R. A. (1981). Astrophys. **247**, 419.
van Breugel, W. J. M., and Heckman, T. M. (1982). In *Proceedings of IAU Symposium No.* 97, edited by D. S. Heeschen and C. M. Wade (Reidel, Dordrecht), p. 61.
van Breugel, W. J. M. (1983). To be published in *Proceedings of the IAU Symposium No. 110.*
van Breugel, W. J. M., Heckman, T. M., Butcher, H., and Miley, G. K. (1983a). Astrophys. J. (in press).
van Breugel, W. J. M., Heckman, T. M., and Miley, G. K. (1983b). Astrophys. J. (in press).
Wilkinson, P. N. (1982). In *Proceedings of IAU Symposium No. 97,* edited by D. S. Heeschen and C. M. Wade (Reidel, Dordrecht), p. 149.
Wills, B. J., and Wills, D. (1979). Private communication in Phillips, R. B., and Mutel, R. L. (1980). Astrophys. J. **236**, 89.
Wilson, A. S., and Ulvestad, J. S. (1983). Preprint.
Wilson, A. S., and Willis, A. G. (1980). Astrophys. J. **240**, 429.